Ionics (2016) 22:2067–2073
DOI 10.1007/s11581-016-1747-5

ORIGINAL PAPER

Lithium-rich layered nickel–manganese oxides as high-performance cathode materials: the effects of composition and PEG on performance

Meifeng Chen[1] · Wan Ren[1] · Yijia Shao[1] · Ting Shu[1] · Lina Liu[1] · Shijun Liao[1]

Received: 28 April 2016 / Revised: 16 May 2016 / Accepted: 26 May 2016 / Published online: 18 June 2016

Abstract Lithium-rich layered nickel–manganese oxide (LRL-NMO) as a cathode material for rechargeable lithium-ion batteries was successfully prepared using an oxalic acid co-precipitation method, with polyethylene glycol (PEG1000) as an additive. The effects of the Ni/Mn ratio and of PEG on the phase purity, morphology, and electrochemical performance of LRL-NMO were investigated with X-ray diffraction, scanning electron microscope, electrochemical impedance spectroscopy, and charge/discharge testing. $Li[Li_{0.167}Ni_{0.25}Mn_{0.580}]O_2$ delivered the best electrochemical performance among the various $Li[Li_{1/3-2x/3}Ni_xMn_{2/3-x/3}]O_2$ $(0 < x < 0.5)$ materials. Furthermore, the sample to which an appropriate amount of PEG had been added showed much smaller and more uniform particle size, higher discharge capacity and energy density, better cycling stability, and lower resistance. The material prepared by adding 9 wt% PEG exhibited high discharge capacity and stability; after 100 cycles at 2 C, it still delivered a discharge capacity of 125.6 mAh g^{-1}, which was 50 % higher than that of a sample prepared without PEG.

Keywords Polyethylene glycol · Lithium-rich layered oxide · Cathode materials · Lithium-ion battery

✉ Shijun Liao
chsjliao@scut.edu.cn

[1] The Key Laboratory of Fuel Cell Technology of Guangdong Province & The Key Laboratory of New Energy Technology of Guangdong Universities, School of Chemistry and Chemical Engineering, South China University of Technology, Guangzhou 510641, China

Introduction

With the rapid development of electric vehicles, the demand for high-energy, high-power lithium-ion batteries has become increasingly urgent [1, 2]. The cathode material is one of the most important components in a lithium-ion battery, playing a major role in its performance, safety, and stability. Current cathode materials are not satisfactory because they have relatively low capacity and poor cycling stability [3]. Recently, layered lithium nickel–manganese oxides, $Li[Li_{1/3-2x/3}Ni_xMn_{2/3-x/3}]O_2$ $(0 < x < 0.5)$, have received increasing attention because their theoretical discharge capacity is over 250 mAh g^{-1}, making them attractive alternative cathode materials for use in electric vehicles [4–6]. A lot of research on $Li[Li_{1/3-2x/3}Ni_xMn_{2/3-x/3}]O_2$ materials with various ratios of Ni to Mn has been reported recently, such as that of Cheng et al. [7] which reported the synthesis of a layered $Li_{1.2}Mn_{0.6}Ni_{0.2}O_2$ cathode material which exhibited a 250-mAh g^{-1} discharge capacity at the first cycle and a good rate capability. Xiang et al. [6] prepared a $Li[Li_{0.131}Ni_{0.304}Mn_{0.565}]O_2$ material through a co-precipitation method. The material exhibited good stability during the cycles with uniform particle size. Wang et al. [4] found that the material $Li_{1.13}Ni_{0.3}Mn_{0.57}O_2$ had good electrochemical stability with a reversible capacity of about 200 mAh g^{-1}. Clearly, the ratio of Ni to Mn, or the content of Ni, affected the properties of the materials significantly; however, there is no systematic investigation on this issue reported up to now. Thus, it is necessary to further explore the effects of Ni contents on the structure and electrochemical performance of $Li[Li_{1/3-2x/3}Ni_xMn_{2/3-x/3}]O_2$ cathode materials.

On the other hand, this material's low coulombic efficiency in the first cycle, poor rate performance, and low tap density have limited its development. To overcome these problems, many researchers have tried to improve its electrochemical performance

by doping it with ions [8, 9], coating it with other materials [10], or controlling its particle size [11]. Polymers (including PAA [12], PVP [13], PPy [14], and PEG [15]) have also been added during the preparation process to improve its structure and morphology, with consequent improvements in performance.

Due to its aqueous solubility, dispersion, and level of viscosity, polyethylene glycol (PEG) has been proven to be a good additive for improving the electrochemical performance of some cathode materials. Yang et al. [16] synthesized $LiFePO_4$ (or LFP) nanoparticles using a solvothermal method in a water–PEG mixture; they found that adding PEG changed the topography of $LiFePO_4$ (reducing the particle size from 1 μm to 200 nm), and the capacity retention rate remained at 89 % after 1000 cycles at 20 C Lu et al. [17] prepared $LiNi_{2/3}Mn_{1/3}O_2$ as a cathode material using PEG400 as the template. With the proper amount of PEG, the obtained sample showed improved cyclic performance and rate capability, which was attributable to low Li/Ni cation disorder, good crystallization, and uniform morphology—all due to the PEG.

Inspired by these previous efforts, we used PEG as an additive in the preparation of lithium-rich layered nickel–manganese oxide (LRL-NMO) and found that PEG significantly enhanced the material's electrochemical performance. The particle size became smaller and the particle size distribution more uniform, the discharge capacity was much better, and the discharge voltage platform was more stable.

Experimental

Materials synthesis

All of the materials were synthesized by a co-precipitation method. The typical procedures were as follows. First, a certain amount of PEG was dissolved in deionized water, then 4.3076 g manganese acetate tetrahydrate ($Mn(CH_3COO)_2{\cdot}4H_2O$, 99.0 %, Kermel) and 1.9045 g nickel acetate tetrahydrate ($Ni(CH_3COO)_2{\cdot}4H_2O$, 98.0 %, Kermel) were added to the PEG solution. An oxalate co-precipitate of Mn and Ni was obtained by the dropwise addition of 4.0809 g oxalic acid dihydrate ($C_2H_2O_4{\cdot}2H_2O$, 99.5 %, Enox), followed by aging, washing, and filtering, then drying overnight. The precipitate was then calcined at 550 °C for 5 h to obtain a binary oxide. Finally, the binary oxide was mixed with 1.4668 g lithium carbonate (Li_2CO_3, 97.0 %, Kermel) and then ball-milled for 2 h, followed by calcining at 900 °C in air for 15 h to obtain about 2.5 g $Li[Li_{0.167}Ni_{0.25}Mn_{0.580}]O_2$ [18].

For comparison, we prepared samples using the same procedures, but without PEG.

Material characterization

The crystal structure of the materials was characterized on a TD-3500 powder diffractometer (Tongda, China) operated at 40 kV and 30 mA using CuK_α as the radiation source. The particle size and morphology of the samples were examined using a Nova NanoSEM 430 scanning electronic microscope (SEM, Philips, the Netherlands). Thermogravimetric analysis was performed on a Q600 SDT thermal analyzer (TA Inc., USA) in the range of 30–900 °C at a heating rate of 10 K min^{-1} in air.

Electrochemical testing

Charge and discharge performance measurements were carried out with CR-2016 test cells using a lithium metal plate as the anode, Celgard 2400 single polypropylene as the separator, and 1 M lithium hexafluorophosphate ($LiPF_6$) solution (EC/DMC = 1:1 in solvent) as the electrolyte. The cathode was prepared by mixing the cathode material with acetylene black and polyvinylidene fluoride using a weight ratio of 85:5:10 in *N*-methyl pyrrolidinone; this mixture was then cast on aluminum foil using the doctor blade technique and dried under vacuum at 80 °C overnight. Then, the electrodes with a diameter of 16 mm (or geometrical area of 2.0 cm^{-2}) were obtained by cutting the material-coated foil with a mold; the loading of the cathode material on the electrode was obtained by weighing the electrode with balance. The charge and discharge measurements were performed galvanostatically on a Neware Battery Testing System (Shenzhen, China) at the desired current density, between 2 and 4.8 V (vs. Li^+/Li) and at room temperature. Electrochemical impedance spectroscopy (EIS) measurements were performed using an IM6e electrochemical workstation (Zahner, Germany). The amplitude of the AC signal was 10 mV over a frequency range of 0.01-10^5Hz. The lithium metal anode served as both counter and reference electrodes during the EIS measurements.

Results and discussion

Optimal metal ratio

$Li[Li_{1/3-2x/3}Ni_xMn_{2/3-x/3}]O_2$ ($0 < x < 0.5$) are generally recognized to be "composite" layered materials of Li_2MnO_3 and $LiNi_{0.5}Mn_{0.5}O_2$. Because the Mn^{4+} in Li_2MnO_3 is further oxidized only with difficulty, Li_2MnO_3 generally exhibits poor electrochemical performance. However, it can display perfect electrochemical performance after being combined with an appropriate amount of $LiNi_{0.5}Mn_{0.5}O_2$. Indeed, the ratio of Li_2MnO_3 to $LiNi_{0.5}Mn_{0.5}O_2$, or the ratio of Mn to Ni, plays an important role in the material's electrochemical performance. To optimize the composition, we prepared a series of samples with various ratios of Mn to Ni, as well as various corresponding ratios of Li to Mn: $Li[Li_{0.263}Ni_{0.10}Mn_{0.633}]O_2$, $Li[Li_{0.233}Ni_{0.15}Mn_{0.617}]O_2$, $Li[Li_{0.200}Ni_{0.20}Mn_{0.600}]O_2$, $Li[Li_{0.167}Ni_{0.25}Mn_{0.580}]O_2$, $Li[Li_{0.133}Ni_{0.30}Mn_{0.567}]O_2$, $Li[Li_{0.110}Ni_{0.35}Mn_{0.550}]O_2$, $Li[Li_{0.106}Ni_{0.40}Mn_{0.533}]O_2$, and $Li[Li_{0.103}Ni_{0.45}Mn_{0.516}]O_2$.

The X-ray diffraction (XRD) patterns of the samples are shown in Fig. 1a. All of the samples can be assigned a $NaFeO_2$ layer structure with space group R-3m, apart from some small peaks found in a 2θ range of 20–25° that belong to space group C2/m. These small peaks are relevant to the $LiMn_6$ cation ordering that occurs in the transition metal layers of Li_2MnO_3. With an increase in the amount of Ni, those small peaks gradually disappear; in other words, the samples with Ni content above 0.35 completely belong to space group R-3m [19]. The sharp splits in (018)/(110) signify a layered structure and good structural compatibility between Li_2MnO_3 and $LiNi_{0.5}Mn_{0.5}O_2$ [20]. However, Fig. 1b shows that the splits in (018)/(110) became increasingly flatter as the amount of Ni rose. The characteristics of the layered structure became less obvious, although this was perhaps simply because the Li_2MnO_3 was formed in the $LiNi_{0.5}Mn_{0.5}O_2$ layer.

To facilitate further understanding of the compound's structure, we list the ratios of I(003)/I(104) in Table 1. Ni^{2+} may have traveled from the transition metal layer to the lithium layer, thereby hindering the path of Li^+ diffusion [17]. Higher ratios of I(003)/I(104), especially above 1.2, have been said to lead to better cationic order. Table 1 shows that all of the ratios were above 1.2, indicating that the samples had a structure that was beneficial for Li^+ diffusion.

Figure 2 shows the discharge curves of $Li[Li_{1/3-2x/3}Ni_xMn_{2/3-x/3}]O_2$ ($0 < x < 0.5$) samples in the voltage range of 2.0–4.8 V at 0.1 C. Their discharge capacities were respectively 125.8, 151.9, 230.7, 243.4, 221.5, 209.5, 213.7, and 204.7 mAh g^{-1} as the amount of Ni increased. Although $Li[Li_{0.103}Ni_{0.45}Mn_{0.516}]O_2$ had the highest discharge flat voltage, $Li[Li_{0.167}Ni_{0.25}Mn_{0.580}]O_2$ showed the highest discharge capacity and a higher discharge flat voltage. In addition, materials with lower Ni content have more commercial value because Ni is environmentally toxic.

In summary, $Li[Li_{0.167}Ni_{0.25}Mn_{0.580}]O_2$ had a higher discharge capacity, a more stable discharge voltage platform, and lower Ni content among the $Li[Li_{1/3-2x/3}Ni_xMn_{2/3-x/3}]O_2$ ($0 < x < 0.5$) materials examined, so we selected it to explore the effect of PEG on the electrochemical performance of Li-rich layered lithium nickel–manganese oxides.

The effect of PEG

Figure 3 shows the analysis curves (thermogravimetric/differential thermal analysis, TG/DTA) of PEG1000 at a heating

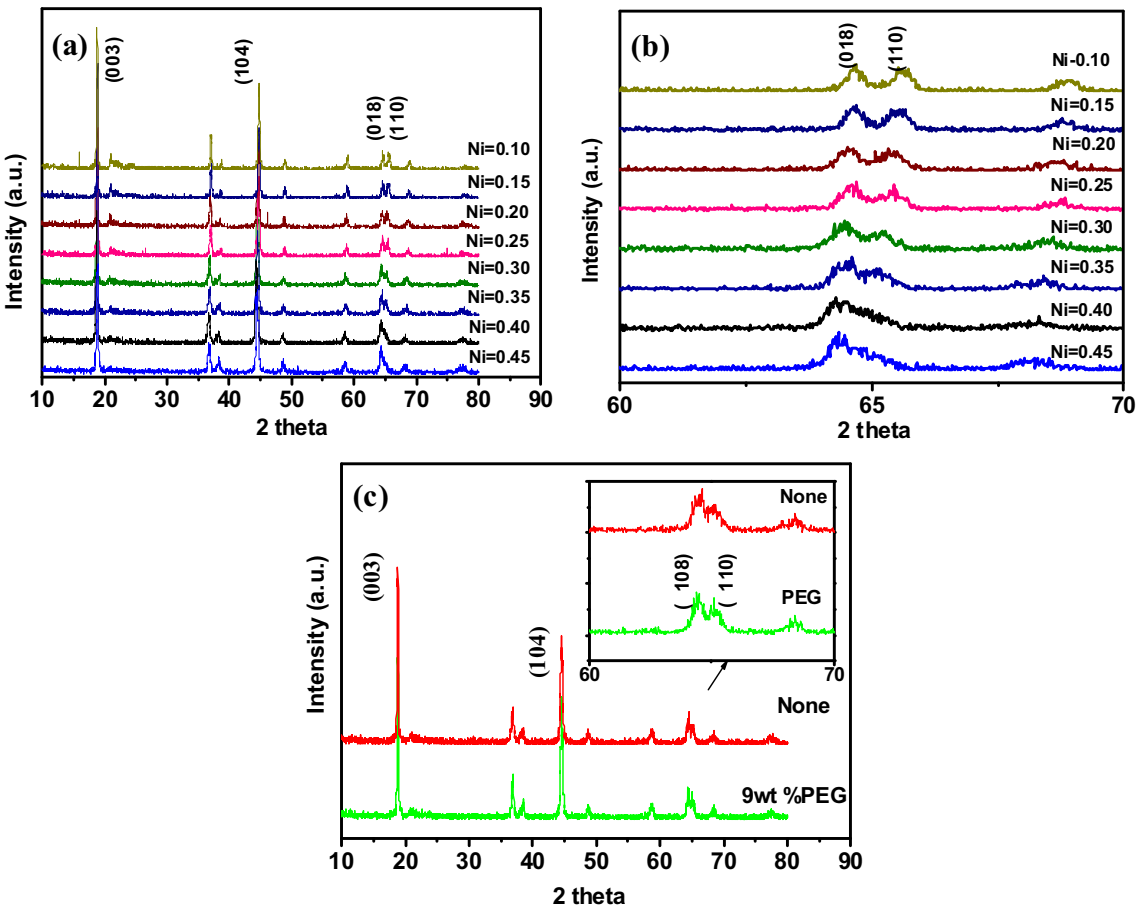

Fig. 1 **a** XRD patterns of the $Li[Li_{1/3-2x/3}Ni_xMn_{2/3-x/3}]O_2$ ($0 < x < 0.5$) samples. **b** An enlargement of (**a**) in the 60–70° region. **c** XRD patterns of bare $Li[Li_{0.167}Ni_{0.25}Mn_{0.580}]O_2$ and 9 wt% PEG-$Li[Li_{0.167}Ni_{0.25}Mn_{0.580}]O_2$

Table 1 Intensity (in arbitrary unit) of (003) and (104) with various metal ratios

Sample	I(003)	I(104)	I(003)/I(104)
$Li[Li_{0.263}Ni_{0.10}Mn_{0.633}]O_2$	2396	1446	1.657
$Li[Li_{0.233}Ni_{0.15}Mn_{0.617}]O_2$	2302	1188	1.938
$Li[Li_{0.200}Ni_{0.20}Mn_{0.600}]O_2$	2435	1489	1.635
$Li[Li_{0.167}Ni_{0.25}Mn_{0.580}]O_2$	2166	1362	1.591
$Li[Li_{0.133}Ni_{0.30}Mn_{0.567}]O_2$	2043	1401	1.458
$Li[Li_{0.110}Ni_{0.35}Mn_{0.550}]O_2$	2307	1413	1.632
$Li[Li_{0.106}Ni_{0.40}Mn_{0.533}]O_2$	2305	1440	1.601
$Li[Li_{0.103}Ni_{0.45}Mn_{0.516}]O_2$	1888	1345	1.403

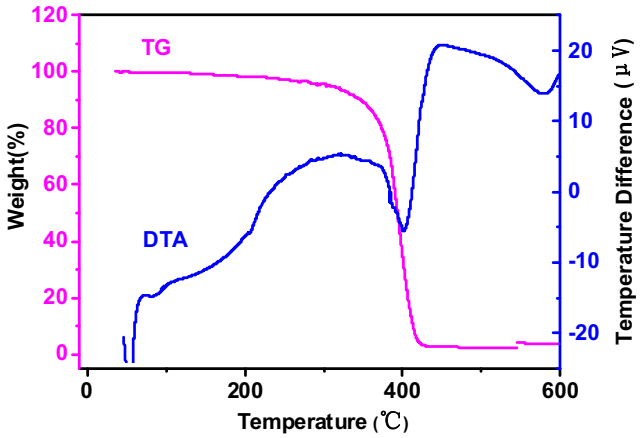

Fig. 3 Thermal gravimetry of PEG1000 (heating rate, 10 K min^{-1})

rate of 10 K min^{-1}. Since PEG1000 was selected as the dispersant, we investigated its thermal behavior using a TGA analyzer. There was an obvious continuous weight loss below 410 °C in the TG curve (reaching approximately 100 %) due to the evaporation of absorbed water and the decomposition of PEG. An endothermic peak appeared at 400 °C—the temperature at which maximum weight loss occurred. Considering the thermal behavior of nickel–manganese oxalate previously reported [21], we set the pre-sintering and post-sintering temperatures at 550 and 900 °C, respectively.

Figure 4a shows the discharge capacity of the samples with different amounts of PEG at various rates between 2 and 4.8 V. The electrochemical performance significantly improved when the PEG content was 9 wt%, but dropped when the PEG content was lower (3 and 6 wt%) or higher (12 wt%). This may have been because a certain amount of PEG induced viscosity, caused special intermolecular forces, and restricted the growth of Ni/Mn oxalate particles. However, an inappropriate amount of PEG might have led to uncontrollable particle growth, resulting in further agglomeration.

The discharge curves of PEG-$Li[Li_{0.167}Ni_{0.25}Mn_{0.580}]O_2$ samples at 2 C are shown in Fig. 4b. The discharge capacities decreased drastically when the amount of PEG was 3, 6, or 12 wt%. Although the discharge capacity increased only a little with 9 wt% PEG, the discharge voltage was about 0.5 V higher than that of the material without PEG; hence, the energy density improved significantly after the addition of 9 wt% PEG.

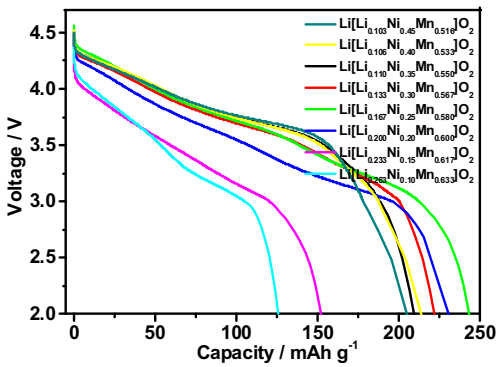

Fig. 2 Discharge curves of $Li[Li_{1/3-2x/3}Ni_xMn_{2/3-x/3}]O_2$ $(0 < x < 0.5)$ samples in the voltage range of 2.0–4.8 V at 0.1 C

We examined the cycling performance of bare $Li[Li_{0.167}Ni_{0.25}Mn_{0.580}]O_2$ and 9 wt% PEG-$Li[Li_{0.167}Ni_{0.25}Mn_{0.580}]O_2$ at discharge rates of 0.5–2 C (Fig. 5a, b). $Li[Li_{0.167}Ni_{0.25}Mn_{0.580}]O_2$ showed excellent performance at both 0.5 and 1 C, with a capacity retention of almost 100 %. But when the discharge rate was raised to 2 C, the discharge capacity dropped to 81.69 mAh g^{-1} at the 100th cycle, and the capacity retention was only 57.76 %. At a high discharge rate, Li^+ would have moved quickly, so the material's structure would have been easily distorted. Hence, having a more stable structure was the key to improving the cycling performance at a high discharge rate. After 9 wt% PEG was added, not only did the capacity at a low discharge rate remain almost the same, but the cycling performance at a high discharge rate (2 C) was also somewhat improved. At 2 C, the discharge capacity of the material with 9 wt% PEG was 120 mAh g^{-1} at the 80th cycle and gradually stabilized by the last 20 cycles. Although the discharge capacity still faded around 30 mAh g^{-1}, the cycling performance was somewhat improved by the addition of PEG.

To clarify the influence of 9 wt% PEG on the electro chemical performance of $Li[Li_{0.167}Ni_{0.25}Mn_{0.580}]O_2$ at the high discharge rate of 2 C, we present in Fig. 5c, d the 10th, 20th, 40th, 60th, 80th, and 100th discharge curves of $Li[Li_{0.167}Ni_{0.25}Mn_{0.580}]O_2$ before and after the addition of 9 wt% PEG. The discharge capacities at different cycles are shown in Table 2. Figure 5c shows that the discharge capacity and midpoint potential both faded quickly after the 20th cycle. Notably, the midpoint potential of the discharge profile at the

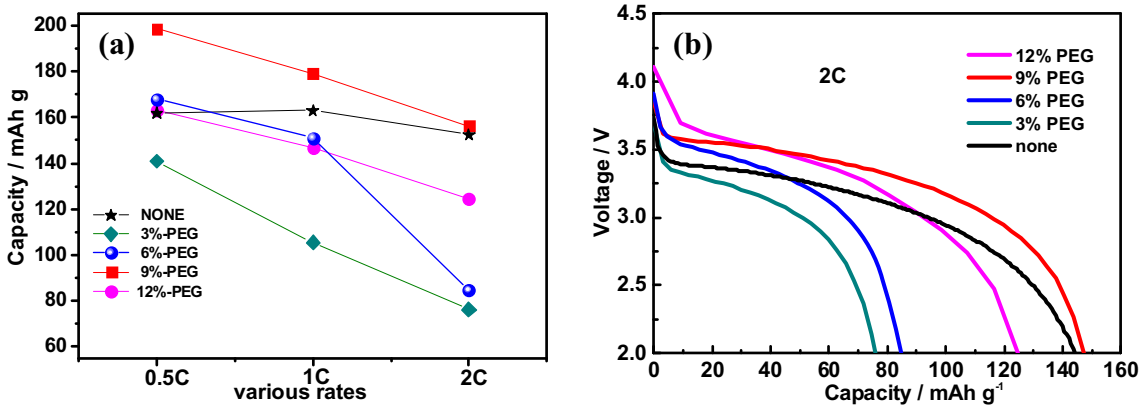

Fig. 4 **a** Discharge capacity of $Li[Li_{0.167}Ni_{0.25}Mn_{0.580}]O_2$ samples with different amounts of PEG at various rates in the voltage range of 2.0–4.8 V. **b** Discharge curves of $Li[Li_{0.167}Ni_{0.25}Mn_{0.580}]O_2$ samples with different amounts of PEG at 2 C

100th cycle was only about 2.6 V. However, after the addition of 9 wt% PEG, the discharge curves remained almost the same up to the 40th cycle. The discharge capacity dropped to 120 mAh g^{-1} at the 80th cycle, but later, the discharge capacity and midpoint potential both gradually stabilized.

In summary, adding 9 wt% PEG had a positive effect on the electrochemical performance of $Li[Li_{0.167}Ni_{0.25}Mn_{0.580}]O_2$. This material had better cycling stability, higher discharge capacity, and greater energy density. To determine what contributed to this material's excellent electrochemical performance, we examined the effect of PEG on the phase purity, morphology, and impedance of $Li[Li_{0.167}Ni_{0.25}Mn_{0.580}]O_2$ using XRD, SEM, and EIS.

The XRD patterns of bare $Li[Li_{0.167}Ni_{0.25}Mn_{0.580}]O_2$ and 9 wt% PEG-$Li[Li_{0.167}Ni_{0.25}Mn_{0.580}]O_2$ are shown in Fig. 1c. The splits in (018)/(110) sharpened and the XRD patterns in the 20–25° 2θ range became flatter after 9 wt% PEG was added. We suggest that 9 wt% PEG-$Li[Li_{0.167}Ni_{0.25}Mn_{0.580}]O_2$ had a better $NaFeO_2$ layer structure, which was beneficial for Li^+ diffusion.

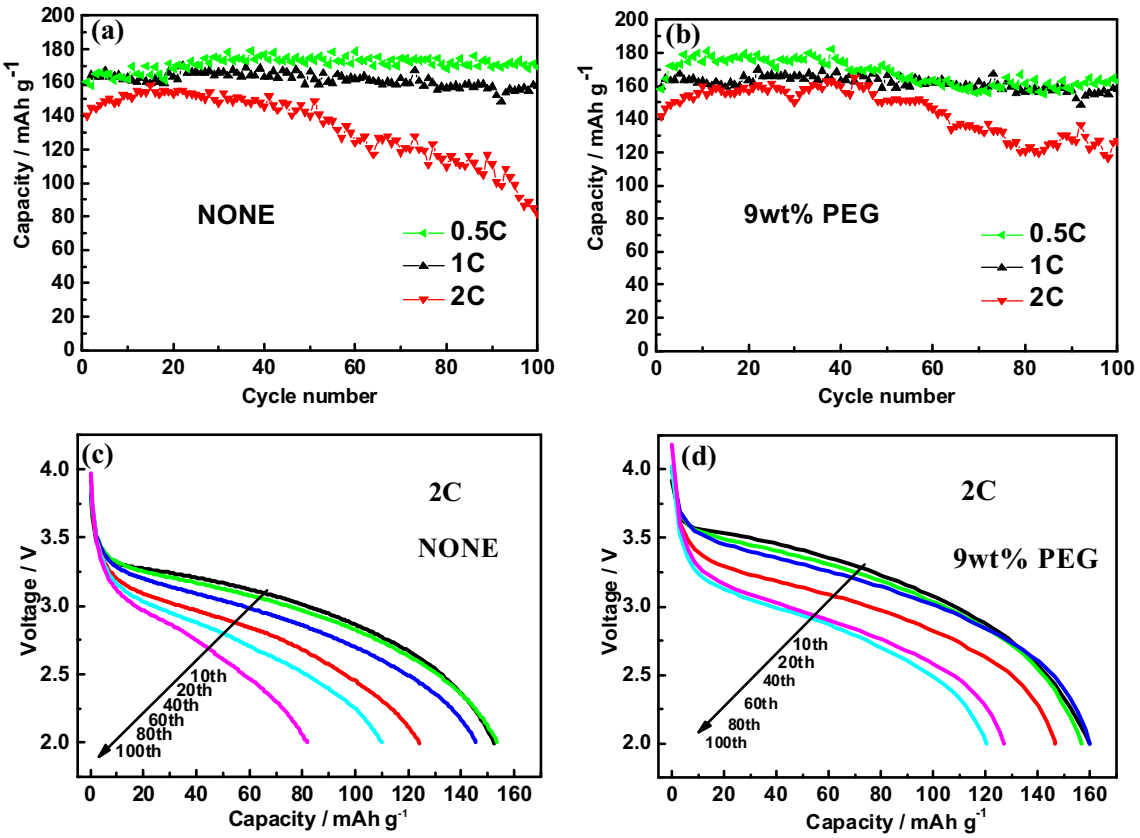

Fig. 5 **a**, **b** Cycling performance of bare $Li[Li_{0.167}Ni_{0.25}Mn_{0.580}]O_2$ and 9 wt% PEG-$Li[Li_{0.167}Ni_{0.25}Mn_{0.580}]O_2$. **c**, **d** Discharge curves of bare $Li[Li_{0.167}Ni_{0.25}Mn_{0.580}]O_2$ and 9 wt% PEG-$Li[Li_{0.167}Ni_{0.25}Mn_{0.580}]O_2$ for different numbers of cycles at 2 C

Table 2 Discharge capacity at different cycles of bare $Li[Li_{0.167}Ni_{0.25}Mn_{0.580}]O_2$ and 9 wt% PEG-$Li[Li_{0.167}Ni_{0.25}Mn_{0.580}]O_2$ at 2 C

Sample	Discharge capacity at different cycles					
	10th	20th	40th	60th	80th	100th
$Li[Li_{0.167}Ni_{0.25}Mn_{0.580}]O_2$	152.3	153.5	145.4	124.1	109.8	81.7
9 wt% PEG-$Li[Li_{0.167}Ni_{0.25}Mn_{0.580}]O_2$	159.6	156.8	159.9	146.4	120.4	126.8

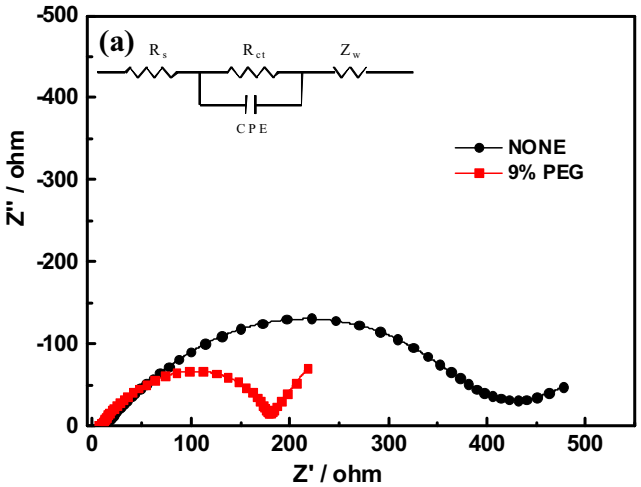

Fig. 6 EIS results of bare $Li[Li_{0.167}Ni_{0.25}Mn_{0.580}]O_2$ and 9 wt% PEG-$Li[Li_{0.167}Ni_{0.25}Mn_{0.580}]O_2$ after 100 cycles at 2 C

Figure 6a presents the Nyquist plots and equivalent circuits for bare $Li[Li_{0.167}Ni_{0.25}Mn_{0.580}]O_2$ and 9 wt% PEG-$Li[Li_{0.167}Ni_{0.25}Mn_{0.580}]O_2$ after 100 cycles at 2 C to study the electrode/electrolyte interfacial properties. Both Nyquist plots show one semicircle in the high-frequency region, which is related to the charge transfer process (R_{ct}), and a slope in the low-frequency region, which is attributable to a semi-infinite Warburg diffusion process in the electrode bulk. R_s represents the internal resistivity of the battery, which corresponds to the x value of the first point of the Nyquist plots [4]. The transfer resistance (R_{ct}) of $Li[Li_{0.167}Ni_{0.25}Mn_{0.580}]O_2$ was 424.7 Ω after 100 cycles at 2 C, then dropped to 181.8 Ω with 9 wt% PEG. This indicates the fast interfacial kinetics of 9 wt% PEG-$Li[Li_{0.167}Ni_{0.25}Mn_{0.580}]O_2$ arising from the structural change that occurred after the addition of PEG.

Figure 7a, b presents the morphology of $Li[Li_{0.167}Ni_{0.25}Mn_{0.580}]O_2$ particles with and without 9 wt% PEG. $Li[Li_{0.167}Ni_{0.25}Mn_{0.580}]O_2$ shows a

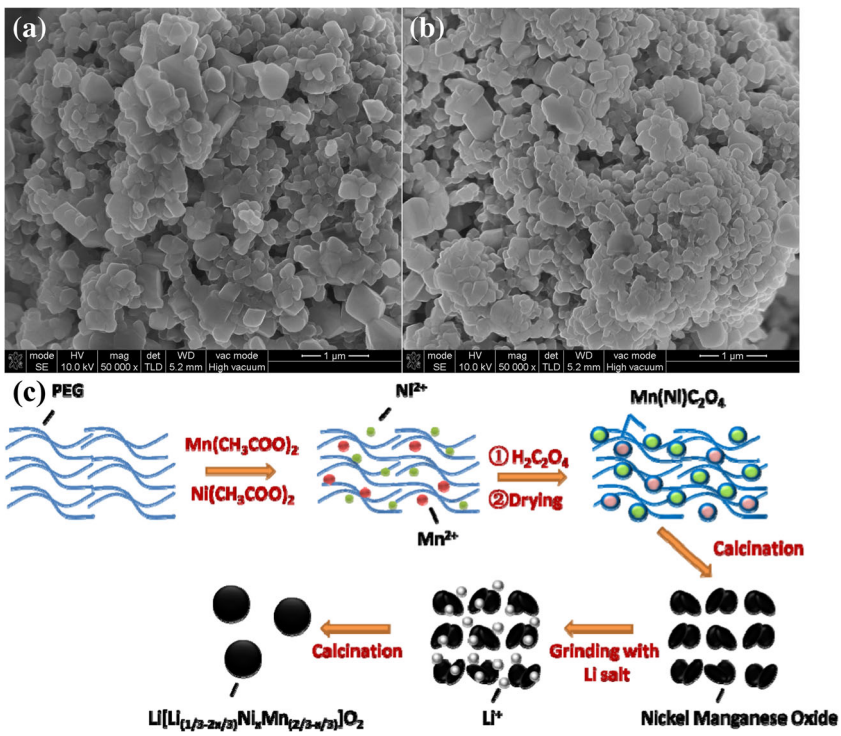

Fig. 7 **a** SEM image of bare $Li[Li_{0.167}Ni_{0.25}Mn_{0.580}]O_2$. **b** SEM image of 9 wt% PEG-$Li[Li_{0.167}Ni_{0.25}Mn_{0.580}]O_2$. **c** Schematic illustration of the formation of PEG-$Li[Li_{1/3-2x/3}Ni_xMn_{2/3-x/3}]O_2$ ($0 < x < 0.5$)

range of particle sizes (Fig. 7a), including more large particles than 9 wt% PEG-Li[$Li_{0.167}Ni_{0.25}Mn_{0.580}$]$O_2$. Hence, this PEG-assisted co-precipitation synthesis method resulted in more uniform particle size and reduced the degree of agglomeration.

Mechanism for the positive effect of PEG

Based on the above TG/DTA results, the weight loss below 410 °C was about 100 % and the post-sintering temperature was set at 550 °C. Thus, we suggest that PEG plays a role in the formation of Mn(Ni)C_2O_4, but not in the final procedure. The schematic illustration of the formation of PEG-Li[$Li_{1/3-2x/3}Ni_xMn_{2/3-x/3}$]$O_2$ ($0 < x < 0.5$) is shown in Fig. 7c. PEG is a good dispersant; nickel and manganese ions disperse uniformly in PEG and results in a uniform nickel–manganese oxalate precipitate, and the final material has a better $NaFeO_2$ layer structure, which is beneficial for Li^+ diffusion. In addition, PEG has high viscosity, which can restrict the growth rate of particles. This synthesis method therefore can yield lithium-rich oxides with a small, uniform particle size, not only shortening the path of Li^+ insertion/desertion but also reducing the transfer resistance within a battery.

Conclusions

In this work, we studied the effect of the Ni/Mn ratio on the electrochemical performance of Li-rich layered lithium nickel–manganese oxides. Among the Li[$Li_{1/3-2x/3}Ni_xMn_{2/3-x/3}$]$O_2$ ($0 < x < 0.5$) materials, Li[$Li_{0.167}Ni_{0.25}Mn_{0.580}$]$O_2$ delivered the highest discharge capacity, had a more stable discharge voltage platform, and had a lower Ni content. We then explored the effect of PEG on the electrochemical performance of Li[$Li_{0.167}Ni_{0.25}Mn_{0.580}$]$O_2$, finding that 9 wt% PEG was the most effective. We also have explained the mechanism of PEG's positive effect.

Acknowledgments This work was supported by the National Natural Science Foundation of China (NSFC project nos. 21276098, 21476088, 51302091, and U1301245), the Natural Science Foundation of Guangdong Province (project nos. 2014A010105041 and 2015A030312007), and the Educational Commission of Guangdong Province (project no. 2013CXZDA003).

References

1. Goodenough JB, Park K-S (2013) The Li-ion rechargeable battery: a perspective. J Am Chem Soc 135:1167–1176
2. Chen JJ (2013) Recent progress in advanced materials for lithium ion batteries. Materials 6:156–183
3. Goodenough JB, Kim Y (2009) Challenges for rechargeable Li batteries†. Chem Mat 22:587–603
4. Wang YH, Bie XF, Nikolowski K, Ehrenberg H, Du F, Hinterstein M, Wang CZ, Chen G, Wei YJ (2013) Relationships between structural changes and electrochemical kinetics of Li-excess $Li_{1.13}Ni_{0.3}Mn_{0.57}O_2$ during the first charge. J Phys Chem C 117:3279–3286
5. Lin J, Mu DB, Jin Y, Wu BR, Ma YF, Wu F (2013) Li-rich layered composite Li[$Li_{0.2}Ni_{0.2}Mn_{0.6}$]O_2 synthesized by a novel approach as cathode material for lithium ion battery. J Power Sources 230:76–80
6. Xiang X, Li X, Li W (2013) Preparation and characterization of size-uniform Li[$Li_{0.131}Ni_{0.304}Mn_{0.565}$]$O_2$ particles as cathode materials for high energy lithium ion battery. J Power Sources 230:89–95
7. Fuquan C, Yuelong X, Jitao C, Li L, Xinxiang Z, Henghui Z (2013) Monodisperse $Li_{1.2}Mn_{0.6}Ni_{0.2}O_2$ microspheres with enhanced lithium storage capability. J Mater Chem A 1:5301–5308
8. Wu Y, Manthiram A (2007) Effect of Al^{3+} and F^- doping on the irreversible oxygen loss from layered Li[$Li_{0.17}Mn_{0.58}Ni_{0.25}$]$O_2$ cathodes. Electrochem Solid-State Lett 10:A151–A154
9. Singh G, Thomas R, Kumar A, Katiyar RS (2012) Electrochemical behavior of Cr-doped composite Li_2MnO_3-$LiMn_{0.5}Ni_{0.5}O_2$ cathode materials. J Electrochem Soc 159:A410–A420
10. Singh G, Thomas R, Kumar A, Katiyar RS, Manivannan A (2012) Electrochemical and structural investigations on ZnO treated $_{0.5}Li_2Mn_{O3}$-$_{0.5}LiMn_{0.5}Ni_{0.5}O_2$ layered composite cathode material for lithium ion battery. J Electrochem Soc 159:A470–A478
11. Kim JH, Choi SH, Son MY, Kim MH, Lee JK, Kang YC (2013) Electrochemical properties of nanometer-sized 0.6Li(2)MnO(3) center dot 0.4LiNi(0.5)Mn(0.5)O(2) composite powders prepared by flame spray pyrolysis. Ceram Int 39:331–336
12. Zhao CH, Kang WP, Xue QB, Shen Q (2012) Polymerization-pyrolysis-assisted nanofabrication of solid solution $Li_{1.2}Ni_{0.13}Co_{0.13}Mn_{0.54}O_2$ for lithium-ion battery cathodes. J Nanopart Res 14:1240
13. Lim S, Cho J (2008) PVP-functionalized nanometre scale metal oxide coatings for cathode materials: successful application to $LiMn_2O_4$ spinel nanoparticles. Chem Commun (Camb) 37:4472–4474
14. Orinakova R, Fedorkova A, Orinak A (2013) Effect of PPy/PEG conducting polymer film on electrochemical performance of $LiFePO_4$ cathode material for Li-ion batteries. Chem Pap 67:860–875
15. Fedorková A, Nacher-Alejos A, Gómez-Romero P, Oriňáková R, Kaniansky D (2010) Structural and electrochemical studies of PPy/PEG-$LiFePO_4$ cathode material for Li-ion batteries. Electrochim Acta 55:943–947
16. Yang S, Zhou X, Zhang J, Liu Z (2010) Morphology-controlled solvothermal synthesis of $LiFePO_4$ as a cathode material for lithium-ion batteries. J Mater Chem 20:8086
17. Lu Y-X, Jiang Y, Yang Z, Han J-T, Huang Y-H, Ma J (2013) Polymer-assisted synthesis of $LiNi_{2/3}Mn_{1/3}O_2$ cathode material with enhanced electrochemical performance. J Alloy Compd 559:203–208
18. Ren W, Luo R, Liu Z-s, Tan X-y, Fu Z-y, Liao S-j (2014) Effect of Ni/Mn ratio on the performance of $LiNi_xMn_{2-x}O_4$ cathode material for lithium-ion battery. Ionics 20:1361–1366
19. Yabuuchi N, Yamamoto K, Yoshii K, Nakai I, Nishizawa T, Omaru A, Toyooka T, Komaba S (2013) Structural and electrochemical characterizations on Li_2MnO_3-$LiCoO_2$-$LiCrO_2$ system as positive electrode materials for rechargeable lithium batteries. J Electrochem Soc 160: A39–A45
20. Jing L, Daobin M, Ying J, Borong W, Yunfeng M, Feng W (2013) Li-rich layered composite Li[$Li_{0.2}Ni_{0.2}Mn_{0.6}$]O_2 synthesized by a novel approach as cathode material for lithium ion battery. J Power Sources 230:76–8080
21. Liu Z, Jiang Y, Zeng X, Xiao G, Song H, Liao S (2014) Two-step oxalate approach for the preparation of high performance $LiNi_{0.5}Mn_{1.5}O_4$ cathode material with high voltage. J Power Sources 247:437–443